PbSe Nanorod Field-Effect Transistors

Han, Lu; Balazs, Daniel M.; Shulga, Artem G.; Abdu-Aguye, Mustapha; Ma, Wanli; Loi, Maria Antonietta

Published in:
Advanced electronic materials

DOI:
10.1002/aelm.201700580

Publication date:
2018

ADVANCED ELECTRONIC MATERIALS
www.advelectronicmat.de

PbSe Nanorod Field-Effect Transistors: Room- and Low-Temperature Performance

Lu Han, Daniel M. Balazs, Artem G. Shulga, Mustapha Abdu-Aguye, Wanli Ma, and Maria Antonietta Loi**

Lead chalcogenides with large exciton Bohr radius display strong quantum confinement, which make them applicable in a wide range of optoelectronic devices such as solar cells and photodetectors. Especially, 1D PbSe nanocrystals attract much attention with their potential for multiple exciton generation. However, very little is known on their charge transport properties. In this study well performing field-effect transistors based on PbSe nanorods with an inorganic iodide-based ligand are presented for the first time. The transistors at room temperature display ambipolar characteristics with electron mobility of ≈0.1 $cm^2 V^{-1} s^{-1}$ and hole mobility of 1.1×10^{-4} $cm^2 V^{-1} s^{-1}$ in the ultraclean environment. Low temperature investigation reveals a transition around 200 K between nearest-neighbor and variable-range hopping mechanism. Below 200 K, the transport properties are dominated by the severe disorder.

1. Introduction

Colloidal semiconductor quantum dots (QDs) have obtained great interest for their potential application in electronic and optoelectronic devices for their low-cost synthesis methods, size- and shape-tunability, and solution-based processability. These applications include solar cells,[1,2] photodetectors,[3] light-emitting diodes,[4] and field-effect transistors (FETs).[5,6] Compared to bulk materials, colloidal QDs exhibit unique size- and shape-dependent electronic and optical properties associated with quantum confinement effects. Once the physical size of the material becomes comparable to, or smaller than their Bohr radius, quantum confinement effects emerge, the bandgap energy increases, and discrete energy levels appear in the density of states spectrum. From this point of view, PbSe is of particular interest for its large exciton Bohr radius (46 nm) and equal electron and hole effective masses,[7] which allows to achieve strong confinement even in relatively large particles. Moreover, PbSe has a narrow bandgap (0.28 eV in bulk),[8] with consequent optical activity in the near infrared spectral range[9] and displays a high dielectric constant (ε_m = 23).[10] These versatile characteristics make PbSe QDs promising semiconductor building blocks for photovoltaic devices,[11] electronic circuits,[12] and mid- and near-infrared sensing.[13] Moreover, it has been demonstrated that the dimensionality of the nanostructure, in practice the aspect ratio, allows for tuning the physical properties. For example, quasi-1D PbSe nanorods (NRs) have been reported to exhibit more efficient electron transport,[14] enhanced multiple exciton generation,[15,16] reduced Auger recombination rates,[17] higher absorption coefficient,[18] and longer biexciton lifetime[19] relative to PbSe QDs. More recently, a maximum external quantum efficiency of 122% has been reported in PbSe NR solar cells.[15] Despite the prospects for high-performance PbSe NR solar cells,[15,20] there is still a lack of studies about their transport properties. This is especially surprising as due to their 1D confinement higher mobilities than in QDs can be expected. The fabrication of thin-film FETs is a useful method for studying charge transport properties in solution-processed semiconductors, such as QDs.

During synthesis colloidal QDs are capped with long-alkyl chain ligands, which provide solubility and stability in solution but also suppress charge carrier transport when the QDs are assembled in films. Ligand exchange with short molecules that can decrease the inter-QD spacing and passivate surface traps is essential for the fabrication of high performing devices. The choice of ligands largely depends on the desired QD properties. In early works, amines (especially hydrazine) were used for PbSe QD and nanowire-based transistors.[21,22] To cross-link PbSe QD films, a series of short-chain bifunctional molecules (e.g., 1,2-ethanedithiol,[23] 1,3-benzenedithiol,[24] 3-mercaptopropionic acid[25] etc.) were introduced in device fabrication. Most recently, the use of halide ions (Cl^-, Br^-, I^-) have led to rapid improvements in PbS/PbSe QD solar cell power conversion efficiencies (up to 11.3%) and long-term stability in air.[1,26] The proposed

L. Han, D. M. Balazs, A. G. Shulga, M. Abdu-Aguye, Prof. M. A. Loi
Zernike Institute for Advanced Materials University of Groningen
Nijenborgh 4, Groningen 9747 AG, The Netherlands
E-mail: m.a.loi@rug.nl

L. Han, Prof. W. Ma
Institute of Functional Nano and Soft Materials (FUNSOM)
Soochow University
199 Ren-Ai Road, Suzhou Industrial Park
Suzhou, Jiangsu 215123, P. R. China
E-mail: wlma@suda.edu.cn

The ORCID identification number(s) for the author(s) of this article can be found under https://doi.org/10.1002/aelm.201700580.

DOI: 10.1002/aelm.201700580

reasons for this success are that such halide ligands provide a very good passivation for the QD surface.[27] Moreover, the presence of trap states, which may stem from (i) the synthetic process; (ii) the ligand-exchange during fabrication; (iii) adsorption of molecules (e.g., water and oxygen) at the interface between the active layer and gate dielectric,[28] is responsible for not ideal transport properties. Again, while a large number of papers discuss results on PbS and PbSe spherical QDs,[12,29–33] very little is known on PbSe rods charge transport properties.

In this work, we report about the fabrication and properties of PbSe NR FETs. By using high quality PbSe NRs,[20] forming crack-free thin films with an iodide salt (tetra-*n*-butylammonium iodide, TBAI) as ligand and performing fabrication and characterization in ultraclean environment, we obtained electron-dominated ambipolar transistors with electron mobility of ≈0.1 $cm^2\ V^{-1}\ s^{-1}$, hole mobility of $1.1 \times 10^{-4}\ cm^2\ V^{-1}\ s^{-1}$, and electron I_{ON}/I_{OFF} ratio of 3×10^5. Similarly to other nanomaterials, adsorbates (e.g., water and oxygen) introduce trap states, influencing the charge carrier transport in PbSe NR assemblies. Finally, temperature-dependent measurements were carried out under vacuum in a wide temperature range from 297 to 5 K. The analysis of the carrier mobility versus temperature put in evidence two types of electron hopping mechanism and substantial electronic disorder over the whole temperature range.

2. Results and Discussion

Colloidal PbSe NRs are usually synthesized by using oleic acid (OA) as capping agents for the lead precursor, typically leading to NRs of large diameter (>4 nm).[34,35] Recently, we reported that reducing the diameter of PbSe NRs by using *trans*-2-octenoic acid (*t*-2-OA) and OA as mixed capping agents could improve the photovoltaic performance.[20] Herein, we slightly modified the original recipe and used *trans*-2-decenoic acid (*t*-2-DA) as the single capping agent, which gave rise to well-controlled PbSe NRs (see the Experimental Section for details). The procedure for the synthesis of PbSe NRs is schematically shown in **Figure 1**a. While the anisotropic growth of

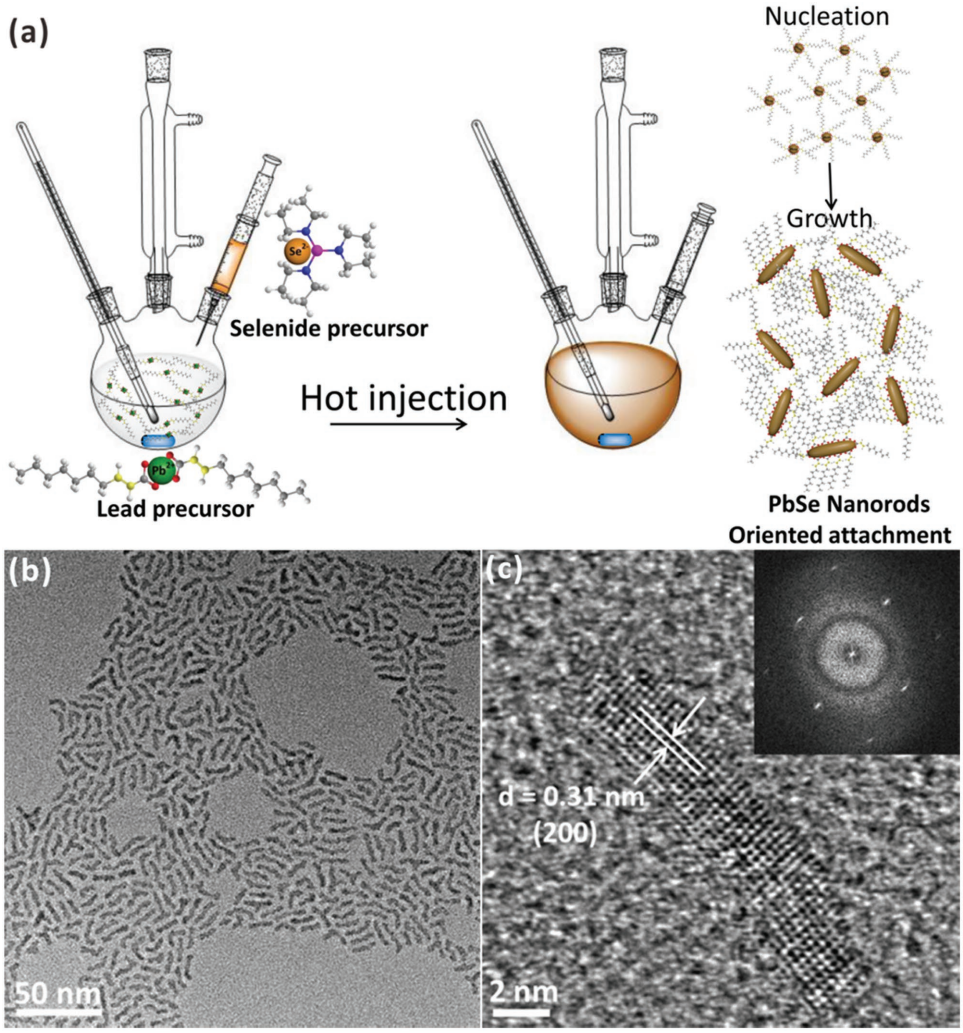

Figure 1. a) Schematics showing the preparation of PbSe NRs. b) TEM image of PbSe NRs just after synthesis. c) HRTEM image of the single PbSe NR with lattice fringes of 0.31 nm. The inset shows the corresponding Fourier transformed image.

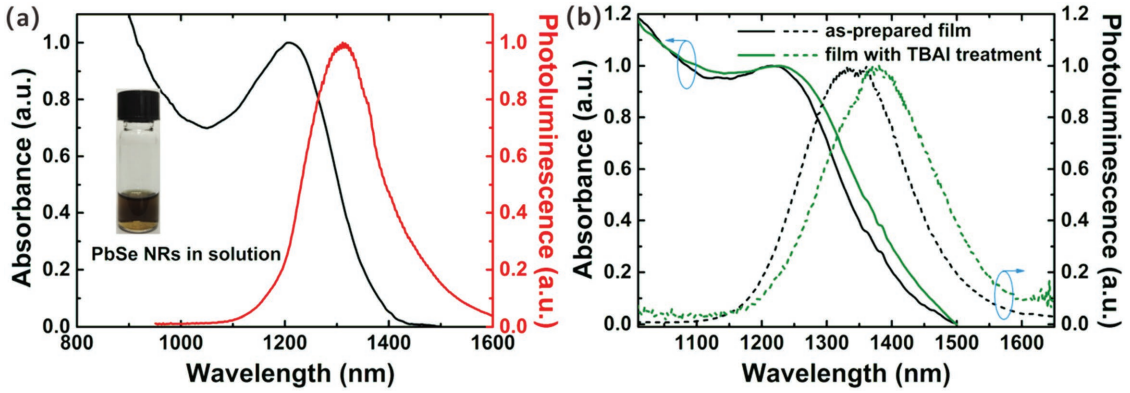

Figure 2. a) Normalized absorbance (black curve) and photoluminescence spectra (red curve) of PbSe NRs in hexane solution. b) Absorption and photoluminescence spectra of as-prepared PbSe NR films (black) and after treatment with TBAI (green).

PbSe nanocrystals is occurring by oriented attachment as previously reported.[20,34] The use of *t*-2-DA, which is two carbon atoms longer than *t*-2-OA, not only decreases the possibility of branched rods but also contributes to increase the solubility of PbSe NRs. A transmission electron microscopy (TEM) image of the synthesized PbSe NRs is shown in Figure 1b, the particles display an average diameter of 2.7 ± 0.2 nm and an average length of 13 ± 3 nm. Figure 1c shows a high-resolution TEM (HRTEM) image of a single PbSe NR showing its good crystallinity and structural integrity. The rod displays atomic planes spaced at 0.31 nm, which corresponds to the (100) planes of the PbSe fcc crystal structure, which is matching the Fourier transform image reported in the inset of Figure 1c.

As-synthesized, PbSe NRs in hexane solution show a well-defined first excitonic absorption peak at 1208 nm, while the photoluminescence (PL) spectra is red-shifted to 1311 nm, as shown in **Figure 2**a. The rather large Stokes shift (about 100 nm) is in agreement with previous studies.[34,36] The position of the first excitonic peak depends on the rod's diameter rather than its length due to the fact that quantum confinement in anisotropic nanostructures is dominated by their smallest length scale.[34,37] To obtain conductive NR solids, we performed ligand exchange on as-deposited layers of NRs using a solution of an organic iodide salt (TBAI). Fourier transform infrared spectroscopy spectra prove the effectiveness of the ligand exchange (Figure S1, Supporting Information). The TBAI-treated films show a flat and uniform surface with a root-mean-square roughness of 1.4 nm, as deduced from atomic force microscopy micrographs (Figure S2a, Supporting Information). Comparing the absorption spectra of PbSe NR films before and after TBAI treatment (Figure 2b), we note that the NR assemblies still preserve the size-dependent optical absorption and emission features after ligand removal, indicating that the exchange process has not compromised the quantum confinement in the resulting films. The red shift between the absorption peak of the as-made films (1214 nm) and the TBAI-treated films (1227 nm) can be explained with the enhanced electronic coupling between NRs after ligand exchange.[23] Such a process reduces the inter-NR distances, in turn leading to increased PbSe NR coupling and conductivity. Similarly, the emission peaks also shifts from 1360 to 1380 nm after ligand exchange, nearly without peak-shape variation. The 153 nm Stokes shift in TBAI treated-films is close to the 146 nm measured in as-made films, but the Stokes shift in both films are significantly larger than that in solution, indicating a probable energy transfer towards NRs of larger diameter. The full width at half maximum of the PL spectra in PbSe NR assemblies (205 nm) show significant broadening with respect to that in solution (164 nm), consistent with the elevate polydispersity of the sample and coupling disorder within the film.[38]

For the FETs fabrication, PbSe NRs were directly deposited on the Si/SiO_2 substrates using a layer-by-layer spin-coating process (**Figure 3**a). The transistor device structure with a bottom gate/bottom contact configuration is depicted in Figure 3b; films of about 40 nm were used as active layer (Figure S2b, Supporting Information). The devices, before electrical characterization in an N_2-filled glovebox were annealed at 120 °C for 30 min to remove the solvent and increase the NR coupling. Typical I_D–V_D output characteristics of the PbSe NR FETs are presented in Figure 3c. The devices show ambipolar behavior with electron-dominated characteristics, and clear current saturation for both n- and p-channel. The I_D–V_G transfer characteristics in the n-channel operation are shown in Figure 3d. Pronounced n-type transport with I_{ON}/I_{OFF} ratio of 10^4 and subthreshold swing (S) value of 3.7 V dec^{-1} is measured. As expected, the hole current shows inferior characteristics with I_{ON}/I_{OFF} ratio of 10^3 and S value of 13.7 V dec^{-1} (Figure S3, Supporting Information). Using Equation (2) (see the Experimental Section), we extracted mobility values of 6.7×10^{-2} cm^2 V^{-1} s^{-1} for electrons, and a much lower mobility of 1.4×10^{-4} cm^2 V^{-1} s^{-1} for holes. To our knowledge, this is the first time that ambipolar FETs based on PbSe NRs with electron mobility higher than 10^{-3} cm^2 V^{-1} s^{-1} are reported.[20] In addition, data of devices of different channel lengths show that the contact resistance does not influence the electron mobility in the linear regime for 20 µm channel length devices (Figures S4 and S5, Supporting Information).

We found that the ambient of measurement plays crucial roles in device performance. The transistors were taken out of the glovebox and were transferred to a vacuum chamber (10^{-7} mbar), where the transistors were again annealed at 120 °C for 30 min. In vacuum the devices retain the ambipolar behavior with electrons being the dominating charge carriers (Figure 3e). However, the performance significantly improved when compared to the characteristics measured in the N_2-filled glovebox

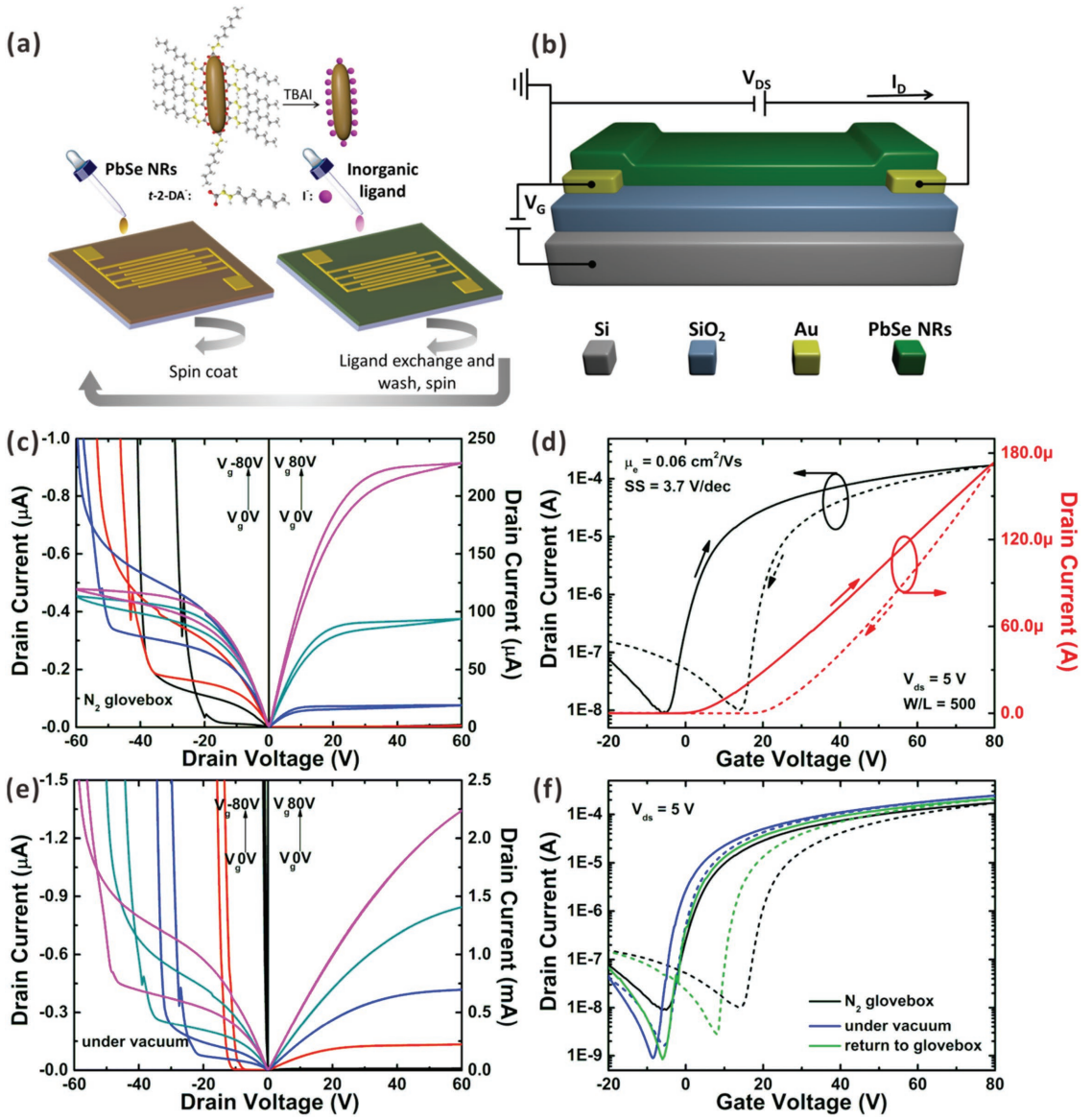

Figure 3. a) A schematic of the spin-coating process used to form PbSe NR films. b) Schematic of the field-effect transistor structure. c) I_D–V_D (output) and d) I_D–V_G (transfer) characteristics of PbSe NR-FETs measured in N_2-filled glovebox. e) I_D–V_D (output) characteristics of the same transistor measured under vacuum at 10^{-7} mbar. f) Comparison of I_D–V_G (transfer) characteristics measured in different environments (solid lines: forward scan and dash lines: reverse scan).

(Figure 3c). For the electron channel, the I_D value linearly increases over a wider V_D range before the saturation regime is reached and a higher linearity of current at low source–drain voltage is observed. To further verify the environmental factors on the device performance, we took the transistors back to the N_2-filled glovebox (before measurement, the transistors were re-annealed at 120 °C for 30 min). The FETs maintain the general ambipolar properties shown earlier. Nonetheless, the saturation currents slightly decrease in the n-channel operation, as seen in Figure S6a in the Supporting Information.

The three corresponding transfer curves to the above mentioned experiments are plotted in Figure 3f and Figure S6b in the Supporting Information. The mobility, I_{ON}/I_{OFF} ratio and S values, and the estimated 2D trap density (see details in the Experimental Section) were extracted in the linear regime of above mentioned transfer curves, and are summarized in **Table 1**. The electron mobility increases under vacuum from 6.7×10^{-2} to 9.2×10^{-2} cm^2 V^{-1} s^{-1} and then decreases to 8.2×10^{-2} cm^2 V^{-1} s^{-1} when back to the glovebox. The hole mobility instead keeps nearly at the same value. The lowest S value of 2.7 V dec^{-1} is observed in vacuum. Herein, the highest electron mobility (around 0.1 cm^2 V^{-1} s^{-1}) using the SiO_2 gate is reported in ambipolar PbSe NR FETs. The value of the electron I_{ON}/I_{OFF} ratio exhibits a tenfold increase after annealing in vacuum and the transistor maintains the high on/off value even back to the glovebox. A similar tendency is observed for the hole I_{ON}/I_{OFF} ratio, but is immediately lost when the sample is back in the glovebox. These observations are in line with a decreased

Table 1. Figures of merits of PbSe NR FETs calculated for different measurement environments.

Surrounding conditions	μ_e [cm^2 V^{-1} s^{-1}]	μ_h [cm^2 V^{-1} s^{-1}]	I_{ON}/I_{OFF} Electron	I_{ON}/I_{OFF} Hole	S [V dec^{-1}] Electron	D_t [cm^{-2} eV^{-1}], $T = 297$ K
N_2 glovebox	6.7×10^{-2}	1.4×10^{-4}	2×10^4	1×10^3	3.7	5.8×10^{12}
Under vacuum	9.2×10^{-2}	1.1×10^{-4}	3×10^5	6×10^4	2.7	4.2×10^{12}
Return to N_2 glovebox	8.2×10^{-2}	1.3×10^{-4}	2×10^5	5×10^3	3.2	5.0×10^{12}

number of electron traps under vacuum. Interestingly, the improvement in electron mobility and in subthreshold swing is partially maintained after the transfer back to the glovebox.

Strongly suppressed hysteresis is observed in the n-channel output and transfer curves in vacuum. The generally observed hysteresis in QD FETs, can be originated from charge transfer to neighboring adsorbates (e.g., water and oxygen), or charge trapping at the dielectric surface or in the active layer.[39,40] In our case, we speculate that annealing in vacuum effectively eliminates adsorbed molecules on the surface of the PbSe NRs, leading to improved electron transport.[41] The hysteresis becomes more pronounced when the sample is returned to the glovebox from the vacuum chamber, but it is still lower than the one measured before the vacuum annealing. It appears that the surface of the NRs reabsorbed gas molecules during the transfer process from/into the glovebox,[22] leading to enhanced hysteresis. However, this adsorption–desorption process appear to be reversible.[25] We calculated the value of the trap density under three different surrounding conditions, as seen in Table 1. The change of the trap density is caused by the gas-adsorption and as expected, the lowest trap density is observed under vacuum. We speculate that electrons easily transfer from PbSe NRs to acceptor states created by molecules bound to the substrate and to the surface of the NRs,[28] which are desorbed upon annealing and vacuum treatments.[25]

In order to better understand the transport mechanism in this NR assembly, the FETs were also characterized at lower temperatures. The temperature-dependent I_D–V_G transfer characteristics measured between 297 and 5 K are displayed in the form of 2D plots (as seen in **Figure 4** and Figure S7, Supporting

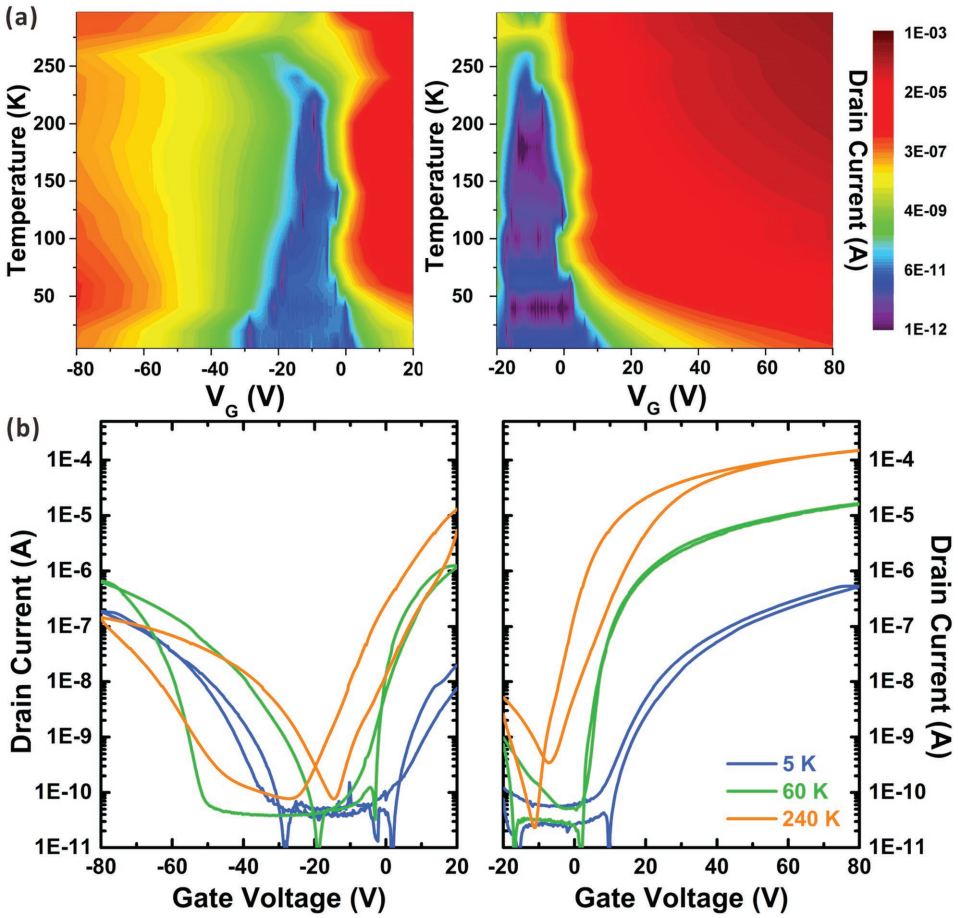

Figure 4. a) Color maps of the forward-scan I_D–V_G (transfer) characteristics at temperatures ranging from 297 to 5 K, measured at –5 and +5 V drain bias, left and right panel, respectively. b) I_D–V_G (transfer) characteristics measured at 5, 60, and 240 K showing the difference in hysteresis measured at –5 and +5 V drain bias, left and right panel, respectively.

Information). The transfer curves exhibit similar ambipolar characteristics dominated by electron transport over the full temperature range. In the n-channel operation, the drain current remarkably increases with the temperature, indicating that electron transport in PbSe NR assemblies is thermally activated (hopping transport).[33] Negligible hysteresis is observed between forward and reverse scan in the n-channel transfer characteristics at temperatures between 240 and 60 K, while a distinct hysteresis appears above 240 K and a small hysteresis is reappearing below 60 K (Figure 4 and Figure S7, Supporting Information). In the p-channel operation, the drain current also increases with increasing temperature with some fluctuation, but the large hysteretic behavior remains over the whole temperature range showing a decrease at low temperature. The temperature behavior of the hysteresis indicates the distribution of the trap states in the semiconductor, in this case showing a broader and deeper trap distribution closer to the highest occupied states of the PbSe rods.

The temperature-dependent I_D–V_D output characteristics exhibit high linearity of the electron current and display clear saturation behavior over the full temperature range (Figure S8, Supporting Information). At very low temperatures (from 40 to 5 K), an injection barrier (appearing as S-shaped output curves at low drain voltages) is observed for both electrons and holes (Figure S9, Supporting Information); hence we excluded these data from the in-depth analysis.

Charge carrier mobilities, I_{ON}/I_{OFF} ratios and subthreshold swing values, as well as trap densities were obtained from the linear regime transfer curves, and are summarized in Table S2 in the Supporting Information. The trap density remains constant in the whole temperature range from 297 to 50 K, indicating deep traps that are active even at room temperature (**Figure 5**a). The ambient-related trap states discussed earlier are expected to lie deep in the bandgap, matching previously observed behavior.[28] The electron and hole I_{ON}/I_{OFF} ratios follow similar trends, as shown in Figure S8b in the Supporting Information. The increase of the I_{ON}/I_{OFF} ratio in the temperature region (from 297 to 220 K) is due predominantly to the decreasing off-current, caused by the decreasing intrinsic carrier density and electron mobility. Subsequently, the I_{ON}/I_{OFF} ratios remain stable between 210 and 50 K and then decrease a lot below 40 K, as a result of the injection-limited on-current. As seen in the 2D images of the transfer characteristics, the voltage onset shifts further from 0 V with the temperature variation, shift that is also visible in the output curves (as seen in Figure S8b,d in the Supporting Information).

The temperature-dependent mobility values obtained from the above described measurements are used to investigate the mechanism of charge transport in PbSe NR assemblies. The temperature dependence of the conductance described as $G = G_0 e^{-\left(\frac{T_0}{T}\right)^p}$, where p depends on the type of hopping and T_0 depends on material properties, which is commonly used to interpret low temperature data of samples where hopping transport is dominant.[42] We can rewrite the above equation as

$$\mu = \mu_0 e^{-\left(\frac{T_0}{T}\right)^p} \rightarrow \ln \mu = \ln \mu_0 - \left(\frac{T_0}{T}\right)^p \quad (1)$$

where μ is the charge carrier mobility, p is the process-dependent hopping exponent and T_0 incorporates both some process and materials properties.[42] The physical content behind the p exponent lies in the details of the hopping process. The probability of a single hopping event between two states can be described as $P \sim \exp\left(-\frac{2r}{a} - \frac{\varepsilon}{k_B T}\right)$, where r is the hopping distance, a is the electron or hole localization length, and ε is the energy difference between the two states involved in the hopping process.[43] In the high temperature range ($2r/a \gg \varepsilon/k_B T$), the energy difference between neighboring sites is not limiting the hopping probability, and thus the dominant process is nearest-neighbor hopping (NNH), with a purely Arrhenius-like behavior ($p = 1$). At low temperatures, on the other hand, the energy difference will be the limiting factor, therefore the hopping will occur between states of similar energies, resulting in a form of variable-range hopping (VRH).[44] In the Mott-type VRH, the p parameter depends on the d dimensionality of the system with $p = 1/(1+d)$. In an FET, the transport occurs in a quasi-2D region at the insulator-semiconductor

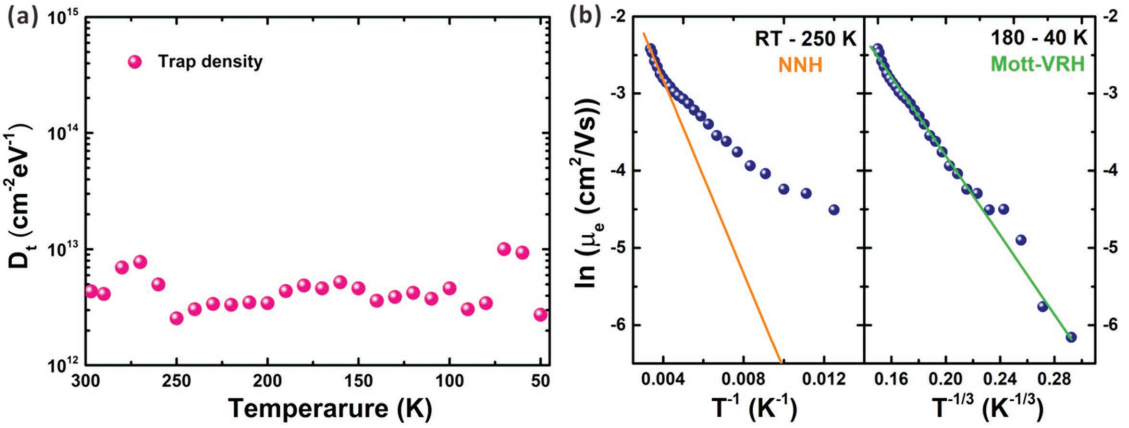

Figure 5. a) Trap densities over the whole temperature range estimated from Equation (3). b) Logarithm of the electron mobility respect to T^{-1} and $T^{-1/3}$ at different temperature ranges, corresponding to nearest-neighbor (NNH) and variable-range hopping (Mott-VRH) mechanisms, respectively. The solid lines are linear fits to the data in the indicated temperature range.

interface, thus $p = 1/3$ is expected. However, in case of large charging energy, a Coulomb-gap appears, giving rise to an exponent $p = 1/2$, called the Efros-Shklovskii (ES)-type VRH.[45] We therefore investigated the dataset by fitting linear functions to plots of $\ln(\mu_e)$ versus T^{-p} with the expected exponents.

The electron mobility shows a monotonic, thermally activated trend, while hole mobility reaches a maximum at intermediate temperatures (as seen in Figure S10c in the Supporting Information). The reasons behind the latter phenomena are unclear and could maybe ascribe to the hole traps. In any case from this point we restrict our analysis to the electron transport. The logarithm of the electron mobility $\ln(\mu_e)$ with respect to T^{-1} and $T^{-1/3}$ are shown in Figure 5b. Between 297 and 250 K the data can be described with a coefficient $p = 1$. This dependence is signature of nearest-neighbor hopping at temperatures where the energy differences between the adjacent states can easily be overcome. In this regime, Equation (1) simplifies to $\mu = \mu_0 e^{\left(-\frac{E_{NN}}{kT}\right)}$; the activation energy of the nearest-neighbor hopping (E_{NN}) was found to be 54 meV. This value matches well the ≈60 meV disorder obtained from the width of the PL peak on the low energy side. In the low temperature region (from 180 to 40 K), the dataset deviates from Arrhenius behavior, and shows a linear dependence with lower p values. Due to the low number of data points, and the unreliability of the data below 40 K, the precise value of the exponent cannot be determined (Figure S11, Supporting Information). Guyot-Sionnest and co-workers described that a transition between the ES- and Mott-VRH is observed with variation of temperature and carrier density.[46] Since we measured the mobilities at rather low carrier densities and the charging energy in our material is expected to be low due to the high dielectric constant, the $p = 1/3$ exponent is the most reasonable result in our case. Moreover, the large disorder shown in the PL data and the NNH-regime of our mobility dataset results in a reduced density of states compared to an ordered system, arguing against the ES-VRH mechanism. In either case, the large electronic disorder dominates the transport properties at low temperatures. In addition, we also observed an apparent $p = 2/3$ regime from 230 to 110 K (Figure S10d, Supporting Information). This exponent has not been reported in CdSe and PbSe QDs, but appeared in ZnO films, where the 2/3 exponent was explained by VRH, which includes activation based on energy fluctuations in the surrounding media.[43] However, at this point it cannot be excluded that 2/3 exponent is due to an artifact caused by a smooth transition between Mott-VRH and NNH, also due to the highly disordered nature of our sample.

3. Conclusion

In summary, we demonstrated that well performing FETs can be fabricated using high quality PbSe NR with TBAI ligands. We found that the measurement environment plays an important role in device performance due to the formation of charge traps by adsorbates (e.g., water and oxygen). Electron mobility of 0.1 $cm^2 V^{-1} s^{-1}$ and n-channel I_{ON}/I_{OFF} ratio of 3×10^5 are achieved in SiO_2 gated-PbSe NR FETs. The temperature-dependent measurements reveal a transition around 200 K between nearest-neighbor and variable-range hopping mechanism. Below this temperature, the transport is dominated by the large disorder, pointing to a possible way of improving the device properties. These results have important implications for further application of PbSe NRs in optoelectronic devices.

4. Experimental Section

Material Preparation: PbSe NRs synthesis was performed with a modified recipe of the one reported in ref. [20] At first, 10 mL tris(diethylamino)phosphine and 10 mmol Se powder were combined and stirred overnight in N_2 glovebox. The synthesis was performed under nitrogen atmosphere using standard air-free Schlenk line techniques. A solution of 89 mg of PbO (1 mmol), 170 mg of *t*-2-DA (1 mmol), and 8 g of 1-octadecene (ODE) was heated at 130 °C in a 50 mL three-neck flask under nitrogen for 1 h. The solution was then degassed at 100 °C for an additional 1 h under vacuum. Subsequently, the solution was kept at 100 °C under nitrogen. A mixture of 1.2 mL 1 M TDPSe and 20 µL diphenylphosphine in 1.2 mL ODE was injected under vigorous stirring. The NRs grew at the injection temperature for 10 min, and the reaction was rapidly quenched by placing the flask in a cold water bath and injecting 5 mL anhydrous hexane. The NRs were purified by precipitation once in hexane/isopropyl alcohol and once in hexane/isopropyl alcohol/acetone and stored in powder form in glovebox.

Characterization: TEM images were recorded on a Tecnai G2 F20 S-Twin transmission electron microscope. UV–vis–NIR spectra were obtained on a UV-3600 model UV–vis–NIR spectrophotometer. For PL measurements, PbSe NRs films were deposited on quartz substrates using the layer-by-layer technique and each layer of carboxylate-capped PbSe NRs was place-exchanged by treating with a solution of 30×10^{-3} M TBAI in anhydrous methanol for 30 s exposure time. The samples were excited with the second harmonic (400 nm) of a mode-locked Ti:Sapphire laser (Mira 900, Coherent). Florescence was collected onto a spectrometer and recorded using an iDus-CCD from Andor Technologies (1.7 µm InGaAs detector). All spectra were corrected for the spectral response of the setup.

Device Fabrication: PbSe NRs FETs were fabricated by a layer-by-layer sequential spin-coating technique on top of the substrate (Figure 3a,b). The configuration of transistor was made on a highly doped silicon substrate with a 230 nm thick SiO_2 layer as gate dielectric, photolithographically patterned gold electrode with 20 µm channel length and 10 mm width. The substrates were cleaned by sonication in acetone, isopropyl alcohol, and acetone for 10 min in sequence and then by plasma treatment for 3 min to remove any organic residue. After cleaning, the substrates were transferred into glovebox for device fabrication. The first thin layer was spin-coated at 1000 rpm for 30 s from 2 mg mL^{-1} solution of *t*-2-DA capped-PbSe NRs in hexane. Solid-state ligand exchange was performed by soaking the as-prepared film in 10×10^{-3} M TBAI solution in methanol for 30 s, followed by two rinse-spin steps with three droplets of acetonitrile. The next three thick layers were spin-coated from 10 mg mL^{-1} solution at 1000 rpm for 30 s, and then soaked into 30×10^{-3} M TBAI solution in methanol for 30 s with the same washing procedure as above. After each spin-coating step and ligand exchange step, the substrate was dried for 5 s at 100 °C on the hot plate. The total thickness of the PbSe NRs film was around 40 nm. The fabrication was completed by annealing the devices for 30 min at 120 °C to remove solvents and improve the NRs binding.

Device Measurements: Transistor measurements were carried out with a Keithley semiconductor characterization system 4200-SCS in combination with a probe station in N_2-filled glovebox. The room-temperature vacuum and temperature-dependent measurements were performed in a probe station (Janis Research, ST-500-2-LF). Measurements were performed under high vacuum (≈10^{-7} mbar) and at varying temperatures between 297 and 5 K using a liquid helium cooling system. The charge carrier mobility (μ) was extracted from

the linear regime of transfer characteristics, using the gradual channel approximation

$$\mu_{\text{lin}} = \frac{L}{WV_{\text{ds}}C_{\text{i}}} \cdot \frac{\partial I_D}{\partial V_G} \quad (2)$$

where L and W are the channel length and channel width respectively, V_{ds} and C_{i} are the dielectric capacitance and source–drain voltage respectively. In the devices, the capacitance of SiO_2 is 15 nF cm^{-2}.

The 2D trap density in the channel, including both the traps at the oxide interface and the bulk traps within the accumulation depth, was estimated from the subthreshold swing using the following formula[47]

$$D_{\text{t}} = \left(\frac{qS}{k_{\text{B}}T\ln 10} - 1\right)\frac{C_{\text{i}}}{q^2} \quad (3)$$

Supporting Information

Supporting Information is available from the Wiley Online Library or from the author.

Acknowledgements

This work was supported by the European Research Council through the ERC Starting Grant "Hy-SPOD" (No. 306983), the National Key Research Projects (Grant No. 2016YFA0202402), the Natural Science Foundation of Jiangsu Province of China (BK20170337), the National Natural Science Foundation of China (Grant No. 61674111), "111" projects and the Priority Academic Program Development of Jiangsu Higher Education Institutions (PAPD). L.H. thanks State-Sponsored Scholarship for Graduate Students from China Scholarship Council (No. 201606920064). The authors kindly thank Arjen Kamp and Teodor Zaharia for the technical assistance and support and Wytse Talsma for assisting temperature-dependent measurements.

Conflict of Interest

The authors declare no conflict of interest.

Keywords

electrical transport properties, field-effect transistors, PbSe nanorods

Received: November 23, 2017
Revised: January 4, 2018
Published online: February 1, 2018

[1] M. Liu, O. Voznyy, R. Sabatini, F. P. Garcia de Arquer, R. Munir, A. H. Balawi, X. Lan, F. Fan, G. Walters, A. R. Kirmani, S. Hoogland, F. Laquai, A. Amassian, E. H. Sargent, *Nat. Mater.* **2017**, *16*, 258.
[2] M. J. Speirs, D. N. Dirin, M. Abdu-Aguye, D. M. Balazs, M. V. Kovalenko, M. A. Loi, *Energy Environ. Sci.* **2016**, *9*, 2916.
[3] F. P. García de Arquer, A. Armin, P. Meredith, E. H. Sargent, *Nat. Rev. Mater.* **2017**, *2*, 16100.
[4] B. S. Mashford, M. Stevenson, Z. Popovic, C. Hamilton, Z. Zhou, C. Breen, J. Steckel, V. Bulovic, M. Bawendi, S. Coe-Sullivan, P. T. Kazlas, *Nat. Photonics* **2013**, *7*, 407.
[5] M. I. Nugraha, R. Hausermann, S. Z. Bisri, H. Matsui, M. Sytnyk, W. Heiss, J. Takeya, M. A. Loi, *Adv. Mater.* **2015**, *27*, 2107.
[6] S. Z. Bisri, C. Piliego, M. Yarema, W. Heiss, M. A. Loi, *Adv. Mater.* **2013**, *25*, 4309.
[7] A. L. Efros, A. L. Efros, *Soviet Physics—Semiconductors* **1982**, *16*, 772.
[8] I. Kang, F. W. Wise, *J. Opt. Soc. Am. B* **1997**, *14*, 1632.
[9] F. W. Wise, *Acc. Chem. Res.* **2000**, *33*, 773.
[10] N. M. Ravindra, V. K. Srivastava, *Phys. Status Solidi A* **1980**, *58*, 311.
[11] J. Zhang, J. Gao, C. P. Church, E. M. Miller, J. M. Luther, V. I. Klimov, M. C. Beard, *Nano Lett.* **2014**, *14*, 6010.
[12] S. J. Oh, Z. Wang, N. E. Berry, J. H. Choi, T. Zhao, E. A. Gaulding, T. Paik, Y. Lai, C. B. Murray, C. R. Kagan, *Nano Lett.* **2014**, *14*, 6210.
[13] H. Talebi, M. Dolatyari, G. Rostami, A. Manzuri, M. Mahmudi, A. Rostami, *Appl. Opt.* **2015**, *54*, 6386.
[14] W. U. Huynh, J. J. Dittmer, A. P. Alivisatos, *Science* **2002**, *295*, 2425.
[15] N. J. Davis, M. L. Bohm, M. Tabachnyk, F. Wisnivesky-Rocca-Rivarola, T. C. Jellicoe, C. Ducati, B. Ehrler, N. C. Greenham, *Nat. Commun.* **2015**, *6*, 8259.
[16] L. A. Padilha, J. T. Stewart, R. L. Sandberg, W. K. Bae, W. K. Koh, J. M. Pietryga, V. I. Klimov, *Acc. Chem. Res.* **2013**, *46*, 1261.
[17] M. Aerts, F. C. Spoor, F. C. Grozema, A. J. Houtepen, J. M. Schins, L. D. Siebbeles, *Nano Lett.* **2013**, *13*, 4380.
[18] P. D. Cunningham, J. E. Boercker, D. Placencia, J. G. Tischler, *ACS Nano* **2014**, *8*, 581.
[19] L. A. Padilha, J. T. Stewart, R. L. Sandberg, W. K. Bae, W. K. Koh, J. M. Pietryga, V. I. Klimov, *Nano Lett.* **2013**, *13*, 1092.
[20] L. Han, J. Liu, N. Yu, Z. Liu, J. Gu, J. Lu, W. Ma, *Nanoscale* **2015**, *7*, 2461.
[21] D. V. Talapin, C. B. Murray, *Science* **2005**, *310*, 86.
[22] S. J. Oh, D. K. Kim, C. R. Kagan, *ACS Nano* **2012**, *6*, 4328.
[23] J. M. Luther, M. Law, Q. Song, C. L. Perkins, M. C. Beard, A. J. Nozik, *ACS Nano* **2008**, *2*, 271.
[24] W. Ma, S. L. Swisher, T. Ewers, J. Engel, V. E. Ferry, H. A. Atwater, A. P. Alivisatos, *ACS Nano* **2011**, *5*, 8140.
[25] D. M. Balazs, M. I. Nugraha, S. Z. Bisri, M. Sytnyk, W. Heiss, M. A. Loi, *Appl. Phys. Lett.* **2014**, *104*, 112104.
[26] C. H. Chuang, P. R. Brown, V. Bulovic, M. G. Bawendi, *Nat. Mater.* **2014**, *13*, 796.
[27] Z. Ning, Y. Ren, S. Hoogland, O. Voznyy, L. Levina, P. Stadler, X. Lan, D. Zhitomirsky, E. H. Sargent, *Adv. Mater.* **2012**, *24*, 6295.
[28] C. M. Aguirre, P. L. Levesque, M. Paillet, F. Lapointe, B. C. St-Antoine, P. Desjardins, R. Martel, *Adv. Mater.* **2009**, *21*, 3087.
[29] M. I. Nugraha, H. Matsui, S. Watanabe, T. Kubo, R. Häusermann, S. Z. Bisri, M. Sytnyk, W. Heiss, M. A. Loi, J. Takeya, *Adv. Electron. Mater.* **2017**, *3*, 1600360.
[30] A. G. Shulga, L. Piveteau, S. Z. Bisri, M. V. Kovalenko, M. A. Loi, *Adv. Electron. Mater.* **2016**, *2*, 1500467.
[31] H. E. Romero, M. Drndic, *Phys. Rev. Lett.* **2005**, *95*, 156801.
[32] S. J. Oh, N. E. Berry, J.-H. Choi, E. A. Gaulding, H. Lin, T. Paik, B. T. Diroll, S. Muramoto, C. B. Murray, C. R. Kagan, *Nano Lett.* **2014**, *14*, 1559.
[33] K. Whitham, J. Yang, B. H. Savitzky, L. F. Kourkoutis, F. Wise, T. Hanrath, *Nat. Mater.* **2016**, *15*, 557.
[34] W. K. Koh, A. C. Bartnik, F. W. Wise, C. B. Murray, *J. Am. Chem. Soc.* **2010**, *132*, 3909.
[35] D. Placencia, J. E. Boercker, E. E. Foos, J. G. Tischler, *J. Phys. Chem. Lett.* **2015**, *6*, 3360.
[36] J. G. Tischler, T. A. Kennedy, E. R. Glaser, A. L. Efros, E. E. Foos, J. E. Boercker, T. J. Zega, R. M. Stroud, S. C. Erwin, *Phys. Rev. B* **2010**, *82*, 245303.
[37] L. Manna, D. J. Milliron, A. Meisel, E. C. Scher, A. P. Alivisatos, *Nat. Mater.* **2003**, *2*, 382.

[38] R. H. Gilmore, E. M. Lee, M. C. Weidman, A. P. Willard, W. A. Tisdale, *Nano Lett.* **2017**, *17*, 893.
[39] H. Wang, Y. Wu, C. Cong, J. Shang, T. Yu, *ACS Nano* **2010**, *4*, 7221.
[40] D. J. Late, B. Liu, H. S. S. R. Matte, V. P. Dravid, C. N. R. Rao, *ACS Nano* **2012**, *6*, 5635.
[41] D. Jariwala, V. K. Sangwan, D. J. Late, J. E. Johns, V. P. Dravid, T. J. Marks, L. J. Lauhon, M. C. Hersam, *Appl. Phys. Lett.* **2013**, *102*, 173107.
[42] P. Guyot-Sionnest, *J. Phys. Chem. Lett.* **2012**, *3*, 1169.
[43] A. J. Houtepen, D. Kockmann, D. Vanmaekelbergh, *Nano Lett.* **2008**, *8*, 3516.
[44] N. F. Mott, *Philos. Mag.* **1969**, *19*, 835.
[45] A. L. Efros, B. I. Shklovskii, *J. Phys. C: Solid State Phys.* **1975**, *8*, L49.
[46] D. Yu, C. Wang, B. L. Wehrenberg, P. Guyot-Sionnest, *Phys. Rev. Lett.* **2004**, *92*, 216802.
[47] S. M. Sze, K. K. Ng, *Physics of Semiconductor Devices*, John Wiley & Sons, Inc., Hoboken, NJ, USA **2006**.